3D analysis of the synaptic organization in the Entorhinal cortex in Alzheimer's disease

Marta Domínguez-Álvaro[1], Marta Montero-Crespo[1,2], Lidia Blazquez-Llorca[1,4], Javier DeFelipe[1,2,3], Lidia Alonso-Nanclares*[1,2,3]

[1]Laboratorio Cajal de Circuitos Corticales, Centro de Tecnología Biomédica, Universidad Politécnica de Madrid, Pozuelo de Alarcón, 28223, Madrid, Spain

[2]Instituto Cajal, Consejo Superior de Investigaciones Científicas (CSIC), Avda. Doctor Arce, 37, Madrid, 28002, Spain

[3]Centro de Investigación Biomédica en Red sobre Enfermedades Neurodegenerativas (CIBERNED), c/Valderrebollo, 5, Madrid, 28031, Spain

[4]Depto. Psicobiología, Facultad de Psicología, Universidad Nacional de Educación a Distancia (UNED), c/Juan del Rosal, 10, Madrid, 28040, Spain

*Correspondence: L. Alonso-Nanclares (aidil@cajal.csic.es)

Laboratorio Cajal de Circuitos Corticales, Centro de Tecnología Biomédica, Universidad Politécnica de Madrid, Pozuelo de Alarcón, 28223, Madrid, Spain

and

Instituto Cajal, Consejo Superior de Investigaciones Científicas (CSIC), Avda. Doctor Arce, 37, Madrid, 28002, Spain

Abstract

The entorhinal cortex (EC) is especially vulnerable in the early stages of Alzheimer's disease (AD). In particular, cognitive deficits have been linked to alterations in the upper layers of EC. In the present report, we performed light microscopy analysis and 3D ultrastructural analyses of synapses in the EC using Focused Ion Beam/Scanning Electron Microscopy (FIB/SEM) to examine possible alterations related to AD. We analyzed 5000 synaptic junctions that were 3D reconstructed, representing the largest 3D ultrastructural study of synapses in the EC of the human brain from cases with AD performed to date. Structural differences were found in the AD tissue at the light microscope level and at the ultrastructural level. These differences may play a role in the anatomical basis for the impairment of cognitive functions in AD.

Keywords

dementia, electron microscopy, FIB/SEM, medial temporal lobe, neuropil, synapse, ultrastructure

Abbreviations

3D: three-dimensional, AD: Alzheimer's disease, Anti-PHF$_{\text{-Tau-AT8}}$: anti-human PHF$_{\text{-Tau}}$ antibody clone AT8, Aβ: amyloid β, AS: asymmetric synapses, CA: *cornu ammonis*, CSR: Complete Spatial Randomness, DG: dentate gyrus, EC: entorhinal cortex, EM: electron microscopy, FIB/SEM: focused ion beam/scanning electron microscopy, KS: Kolmogorov-Smirnov, MW: Mann-Whitney, PB: phosphate buffer, PSD: post-synaptic density, SAS: synaptic apposition surface, SD: standard deviation, sem: standard error of the mean, SS: symmetric synapses, TEC: transentorhinal cortex, V_v: volume fraction

Introduction

Alzheimer's disease (AD) is a progressive neurodegenerative disease which is considered to be the main cause of dementia. The brain of AD cases shows brain atrophy and, at the neuropathological level, the most characteristic findings include the presence of extracellular amyloid-β (Aβ) plaques and intracellular neurofibrillary tangles of filamentous aggregates of hyperphosphorylated tau protein (Alzheimer's Association, 2020). Aβ plaques and neurofibrillary tangles are mostly found in the cerebral cortex, where both their numbers and the proportion of the cortex affected by them increase progressively as the disease advances (Braak and Braak, 1991; Dickson, 1997; Thal *et al.*, 2002). Studies focusing on AD progression have shown that entorhinal cortex (EC) is one of the first brain regions affected by the presence of altered tau protein (Braak and Braak, 1991).

The EC has been shown to be essential for memory functions and spatial navigation (reviewed in Schultz *et al.*, 2015), and alterations in its upper layers have been related to cognitive deficits in AD patients (Van Hoesen *et al.*, 1991; Gomez-Isla *et al.*, 1996). EC is considered to be an interface between the hippocampal formation and a large variety of association and limbic cortices (Lavenex and Amaral, 2000; Solodkin and Van Hoesen, 1996). In particular, the EC is the origin of the perforant pathway (from layers II and III), which provides the largest input source to the hippocampal formation, targeting the ammonic fields (CA) CA1, CA2 and CA3, as well as the dentate gyrus (DG) and subiculum. Specifically, layer II neurons project to CA1 via the trisynaptic circuit, passing through the dentate gyrus (DG) and CA3, while layer III neurons project directly to CA1 in the monosynaptic pathway (Insausti and Amaral, 2012; Kondo *et al.*, 2009). It has been proposed that the trisynaptic pathway is more susceptible to premature degeneration (reviewed in Van Hoesen *et al.*, 2006; Llorens-Martín *et al.*, 2014).

The presence of pathological forms of Aβ and tau proteins in the cerebral cortex of AD cases has been related to neuronal loss, synapse alterations and dendritic spine degeneration (reviewed in Forner *et al.*, 2017; Chen *et al.*, 2019). It has been proposed that synaptic loss affects the subcortical regions and the entorhinal cortex first, and then progresses to other cortical regions (Braak and Braak, 1991; Braak and Del Tredici, 2012, 2020). The loss and dysfunction of synapses have been proposed as the major

structural correlates of the cognitive decline associated with AD (Coleman *et al.*, 2004; Dickson *et al.*, 1995; Selkoe, 2002; Sze *et al.*, 1997). Therefore, deciphering the changes that affect the normal function of synapses may contribute to better understanding of the pathological mechanisms of AD.

In the present study, we performed 3D ultrastructural analysis of layers II and III of the EC using Focused Ion Beam/Scanning Electron Microscopy (FIB/SEM) and specific software that allows the segmentation of synapses in a reconstructed 3D volume (Morales *et al.*, 2011). This technology greatly facilitates the analysis of possible alterations at the synaptic level in AD, as previously shown in the human transentorhinal cortex and the CA1 hippocampal region (Domínguez-Álvaro *et al.*, 2019; Montero-Crespo *et al.*, 2020*b*). Our goal was to investigate the possible synaptic changes occurring in layers II and III of the EC related to AD, not only with regard to numbers, spatial distribution and types of synapses, but also regarding the morphological characteristics of each synapse (shape and size), as well as possible changes in their postsynaptic targets. For this purpose, we performed an analysis of the neuropil from layers II and III of the EC, from eight human brain autopsies (four subjects with no recorded neurological alterations and four AD cases) with short postmortem delays (of less than 3.5h). Since the presence of Aβ plaques is related to a virtual lack of synapses in their vicinity (Blazquez-Llorca *et al.*, 2013), we focused on the neuropil that was free of plaques. We also used stereological methods to assess cortical atrophy of the EC, and possible changes in the volume occupied by different cortical elements (neuronal and glial cell bodies, blood vessels and neuropil) at the light microscope level.

Results

Data regarding the synaptic organization of the human layers II and III from the EC in the four control subjects has been previously published and detailed information can be found therein (Domínguez-Álvaro *et al.*, 2020). What follows are the alterations of synapses in AD cases in comparison with control cases.

Cortical thickness

The mean cortical thickness of the EC was 2.0±0.17 mm (mean±SD) in the control

group and 1.6±0.49 mm in the cases with AD. Although a lower EC cortical thickness in AD cases (approximately 20% lower in AD cases than in control cases) was observed, we did not find a statistically significant difference between the two groups (MW, p = 0.34; Supplementary Table 1).

Volume fraction of cortical elements

In the control group layer II, the values of the estimated volume fraction (Vv) occupied by neuronal somata, glial somata, blood vessels and neuropil were 4.5%, 2.6%, 3.8% and 89.1%, respectively. In the group with AD, these values were 2.6%, 4.6%, 2.3% and 90.5%, respectively. The only statistically significant difference was that of the Vv of glial somata, which was found to be significantly higher in cases with AD (t-test, p=0.03) (Supplementary Tables 2, 3; Supplementary Fig. 1).

In layer III of the control group, the Vv of neuronal somata, glial somata, blood vessels and neuropil were 7.5%, 2.5%, 3.8% and 86.2%. In cases with AD, these values were 2.9%, 4.5%, 4.0% and 88.6%. Statistical comparisons showed a significantly lower Vv of neuronal somata (t-test, p=0.007) in AD (Supplementary Tables 2, 3; Supplementary Fig. 1).

Synaptic Density and AS:SS ratio

A total of 2,019 synapses from AD cases (1,044 synapses in layer II and 1,065 in layer III) were identified and reconstructed in 3D, after discarding incomplete synapses or those touching the exclusion edges of the CF, and the total volume analyzed was 9,006 μm^3 in AD samples (Table 1; Supplementary Table 4). The synaptic density values were obtained by dividing the total number of synapses by the total volume of the CF.

A significantly lower synaptic density (taking both AS and SS together) was observed in AD cases — this value was 40% lower than in control cases in both EC layers. In layer II, we found 0.24 synapses/μm^3 in AD cases and 0.40 synapses/μm^3 in control cases (MW, p=0.03; Supplementary Fig. 2A). In layer III, the mean synaptic density in AD was 0.24 synapses/μm^3 compared to 0.43 synapses/μm^3 found in control cases (MW, p=0.03; Supplementary Fig. 2B; Table 1; Supplementary Table 4).

The ratio of AS to SS was also analyzed and no statistically significant differences were found between the control group and the AD group in any layer (χ^2, p>0.05). In layer II

and III, the AS:SS ratio for the AD cases was very similar to that of the control cases (close to 92:8 in both layers and groups; Table 1; Supplementary Table 4).

Three-dimensional spatial synaptic distribution

Analysis indicates a clear fit to a CSR model, since F, G and K functions closely resemble the theoretical curve that these functions represent, both in the control and the AD cases (Supplementary Fig. 3). That is, the spatial distribution of the synapses fitted a random distribution in all subjects and layers. Furthermore, the estimation of the distance from each synapse to its closest synapse showed that although the mean distance was greater in AD cases in both layer II (811 nm in control; 906 nm in AD; Table 1; Supplementary Table 4) and layer III (823 nm in control, 970 nm in AD; Table 1; Supplementary Table 4), no statistically significant differences were found (MW, $p>0.05$).

Study of the synapse characteristics

Synaptic size

The AD samples did not show differences between layers in the SAS area of AS (MW, $p=0.41$; Table 2; Supplementary Table 5). However, we found significantly larger mean values of SAS area for AS (MW, $p=0.03$) from layer II in AD cases compared to the controls. These differences were not found in SS or in layer III (MW, $p>0.05$; Table 2; Supplementary Table 5).

Analysis of the frequency distributions of the area and perimeter of the AS showed significant differences in the frequency distributions of area in layer II and in the perimeter in layer III (KS, $p<0.0001$), indicating a lower proportion of small SAS area in layer II in AD cases and higher proportions of small SAS perimeter in layer III in AD cases (Supplementary Fig. 4).

Synaptic shape

Most synapses, AS and SS, presented a macular shape in both control and AD cases in layers II and III (>80%), while synapses with more complex shapes (i.e., horseshoe-shaped, perforated or fragmented) were less frequent (Table 3; Supplementary Tables 6, 7). Evaluation of the possible differences between the control and the AD group in layer II showed a slightly higher proportion of horseshoe-shaped AS in AD samples (χ^2, $p = 0.04$; Table 3; Fig. 1B; Supplementary Table 6). Analysis of layer III revealed that

fragmented (χ^2, p=0.0004) and macular (χ^2, p<0.0001) AS were more frequent in the AD group, whereas perforated AS were less frequent in AD cases than in the control individuals (χ^2, p <0.0001; Table 3; Fig. 1C; Supplementary Table 7). Analysis of the SS in layers II and III did not reveal differences between groups (χ^2, p>0.001).

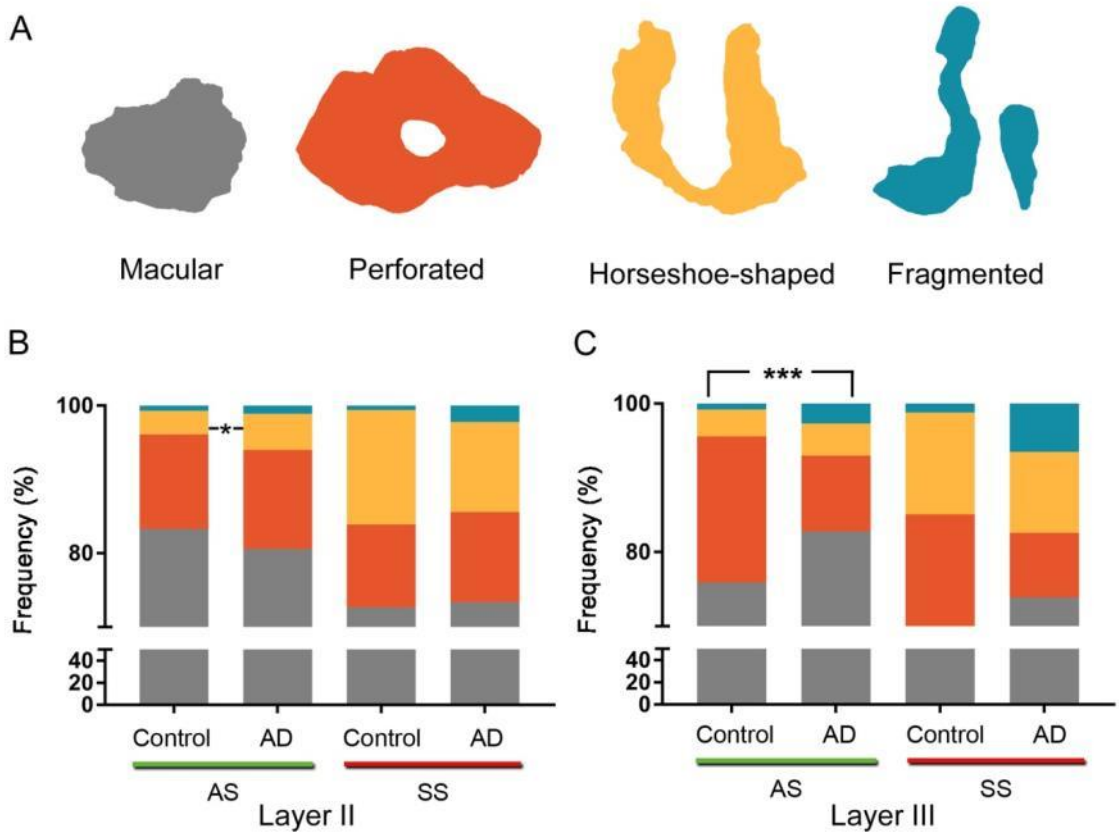

Figure 1. Proportions of the different synaptic shapes (A) in layers II (B) and III (C) of the EC in control subjects and AD patients. (A) Schematic representation of the synaptic shapes: macular synapses, with a continuous disk-shaped PSD; perforated synapses, with holes in the PSD; horseshoe-shaped, with a tortuous horseshoe-shaped perimeter with an indentation; and fragmented synapses, with two PSDs with no connections between them. Proportions of macular, perforated, horseshoe-shaped and fragmented AS and SS are displayed for layer II **(B)** and III **(C)** of the EC in control subjects and AD cases. Statistical differences (indicated with asterisks) showed that in layer II, horseshoe-shaped AS were more frequent (χ^2, p=0.04) in AD cases; and in layer III of the AD group, fragmented (χ^2, p=0.0004) and macular (χ^2, p<0.0001) AS

were more frequent, whereas perforated AS were less frequent in AD cases than in control individuals (χ^2, $p < 0.0001$).

Analysis of Synaptic Size and Shape

Additionally, we determined whether the shape of the synapses was related to their size. For this purpose, the area and perimeter of the SAS of AS were analyzed according to their synaptic shape (SS were not analyzed since the sample size was too small).

When we compared the synaptic size considering the synaptic shape, we found that the mean SAS area from perforated AS in layer III was larger in AD samples (296,156±24,116 nm^2, mean±sem) than in the controls (228,057±6,993 nm^2, mean±sem; MW, $p=0.03$; Supplementary Tables 8, 9). No differences were found in the mean area and perimeter of the SAS from macular, horseshoe-shaped and fragmented synapses (MW, $p>0.05$). Analysis of the frequency distribution of the area and perimeter showed no differences between groups (Supplementary Fig. 5; KS; $p>0.0001$).

Study of the postsynaptic targets

In this study, the postsynaptic targets of 1,538 synapses were determined from the AD samples. In layer II, we identified the postsynaptic targets of a total of 666 AS and 82 SS (Supplementary Tables 10, 11), and in layer III, the postsynaptic targets for 706 AS and 84 SS were determined (Supplementary Tables 10, 12).

As previously described in control EC (Domínguez-Álvaro *et al.*, 2020), the most abundant type of synapse was AS on dendritic shafts (range 45–49%), closely followed by AS on spine heads (39–44%). SS on dendritic shafts were less common (6–9%), SS on spine heads were very uncommon (1%), and AS or SS on spine necks were very infrequent indeed (<1%; Fig. 2). In both controls and AD individuals, excitatory contacts (AS) preferentially targeted dendritic spines, whereas inhibitory contacts (SS) preferentially targeted dendritic shafts (χ^2, $p<0.001$).

Contingency tables were used to assess possible differences in the distribution of postsynaptic elements of cases with AD. No statistically significant differences were found (χ^2, $p>0.001$), although a slightly lower proportion of AS established on spine

heads (χ^2, p=0.02) and a higher proportion of AS on dendritic shafts were observed in AD samples from layer II (χ^2, p=0.03).

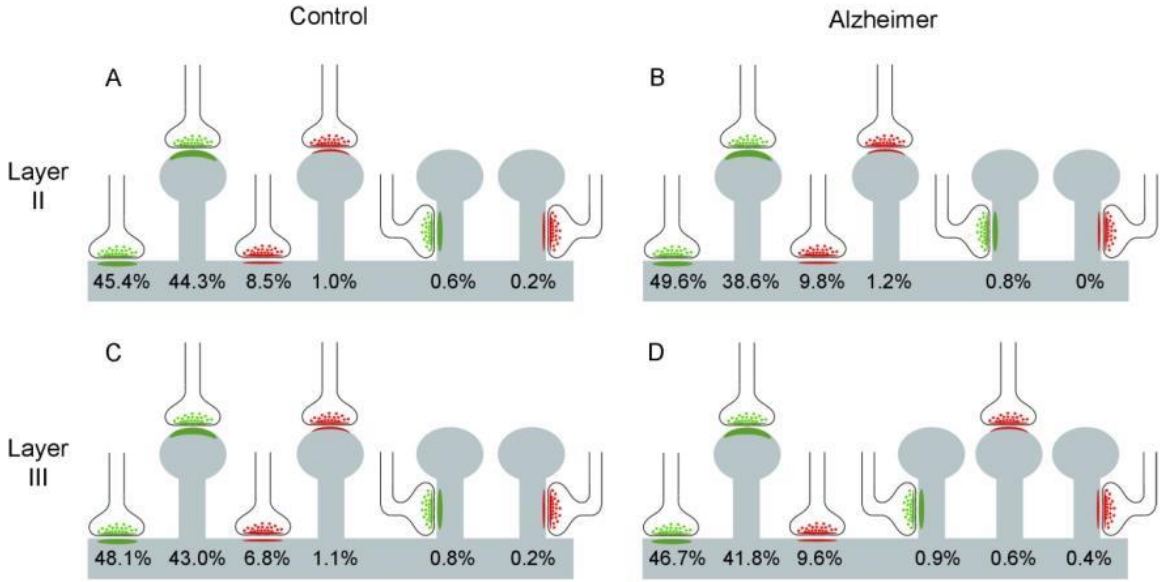

Figure 2. Analysis of the postsynaptic target distribution in layers II (A, B) and III (C, D) of the EC. (A) Schematic representation of the distribution of AS and SS on different postsynaptic targets from control cases in layer II. **(B)** Schematic representation of the distribution of AS and SS on different postsynaptic targets from AD patients in layer II. **(C)** Schematic representation of the distribution of AS and SS on different postsynaptic targets from control cases in layer III. **(D)** Schematic representation of the distribution of AS and SS on different postsynaptic targets from AD patients in layer III. In both layer II and layer III, the AS preferentially targeted spine heads, while the SS preferentially targeted dendritic shafts (asterisks; χ^2, p<0.0001). Percentages of postsynaptic targets are indicated, showing —from left to right— the most frequent type (AS on dendritic shafts) to the least frequent type (SS on spine necks). Synapses on spines have been sub-classified into those that are established on the spine head and those established on the neck.

Finally, we analyzed whether there was a relationship between the synapse size and the type of postsynaptic element with which each of the synapses was established. When

we compared the synaptic size of AS associated with the postsynaptic targets between control cases and AD cases, no differences were found in any layer with regard to the area and perimeter of the SAS (MW, $p>0.05$) or their frequency distribution (KS, $p>0.001$; Supplementary Fig. 6).

Discussion

In total, there are five main findings in the present study: at the light microscope level, (i) cortical thickness was 20% smaller in AD than in control individuals; (ii) a significantly lower volume fraction occupied by neuronal bodies in the layer III was found in AD cases; at the ultrastructural level, (iii) a significantly lower synaptic density was found in both layers in AD cases; (iv) synaptic morphology analysis revealed larger and more complex synapses in layer II in AD cases; and (v) there was a greater proportion of small and simple synapses in layer III in AD cases than in control individuals.

Cortical thickness and volume fraction analysis

At the light microscopic level, atrophy of the EC and adjacent cortical regions is clearly visible to the naked eye (Fig. 3). However, the difference in the mean cortical thickness was less evident (Supplementary Table 1). Macroscopic atrophy of the EC has been described in AD cases (Van Hoesen *et al.*, 1991). This cortical atrophy and, more specifically, the neuronal loss (see below) observed in AD cases have been related to the presence of neurofibrillary tangles (NFTs) and Aβ plaques, with reports indicating an inverse relationship between the number of neurons and the degree of neuropathology (Gómez-Isla *et al.*, 1996; Van Hoesen *et al.*, 1991).

In both layers from the AD brain samples, we found a lower neuronal volume fraction — a difference that was significant in the case of layer III. This is in line with the reported neuronal loss from AD cases in the EC, where the neuronal loss seems to be greater in layers II and IV (Gómez-Isla *et al.*, 1996; Price *et al.*, 2001; Šimić *et al.*, 1997; Van Hoesen and Hyman, 1990). Since the neurons of EC layer III constitute the projection elements of the perforant pathway to the hippocampal CA1 (together with neurons from layer II), this neuronal loss may contribute to the memory impairment

described in AD cases (Andrade-Moraes *et al.*, 2013; Gunten *et al.*, 2006; Hyman *et al.*, 1986; Van Hoesen *et al.*, 1991).

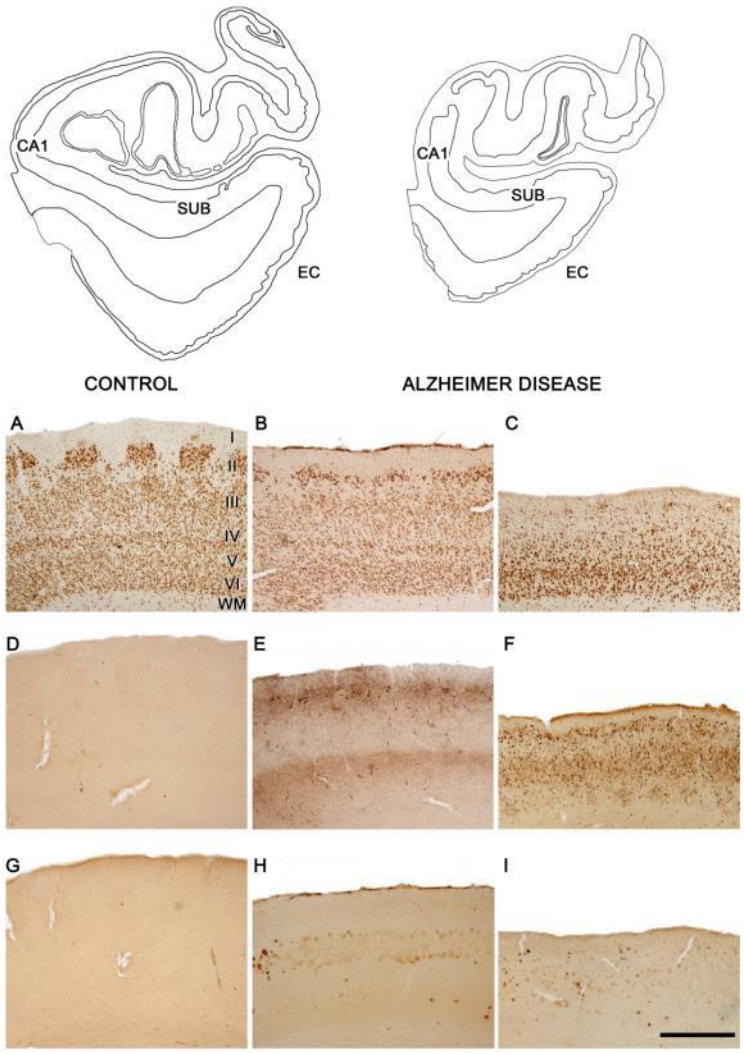

Figure 3. Entorhinal cortex of control and AD cases. (Top) Plots of the medial structures including the hippocampal formation and EC from control (left) and AD (right) cases to illustrate the atrophy that occurs in AD. Plots are based on Nissl-stained coronal sections from cases AB3 and IF1. **(A–I)** Microphotographs showing the EC in a control case AB3 **(A, D, G)** and in AD cases IF1 **(B, E, H)** and VK16 **(C, F, I)**. Layers are indicated to the right of panel **A**. Sections are immunostained with antibodies anti-NeuN **(A–C)**, anti-PHF-Tau-AT8 **(D–F)** and anti-Aβ **(G–I)**. Note the intense labeling of PHF-Tau-AT8 positive neurons (E, F) and Aβ positive plaques (H, I) in AD cases, particularly in case VK16, and the lack of labeling in the control case. CA1: cornu

ammonis field 1; EC: entorhinal cortex; SUB: subiculum; WM: white matter. Scale bar (in I): 4.4 mm in plots and 1 mm in A–I.

The significantly higher volume fraction occupied by glial somata found in layer II is in line with previous reports showing a larger density of glial cells in human EC from AD cases (Muramori *et al.*, 1998). However, no significant differences were found in layer III, suggesting a layer-selective change. The effects of gliosis during AD development are still under debate. It has been proposed that gliosis mediates an inflammatory response to prevent the progression of the disease but that this response may in fact contribute to neurodegeneration (reviewed in Fakhoury, 2018).

Synaptic changes in AD

Synaptic density, proportions and spatial distribution

Our main finding was a significantly lower synaptic density (around 40% lower) in the neuropil of both layer II and layer III of AD individuals compared to controls.

In brain tissue samples from individuals with AD, a lower density of synapses has been described compared to controls in numerous cortical regions, including the DG and certain frontal, parietal, temporal and cingulate cortical areas (Scheff and Price, 1993, 1998, 2003, 2006; Scheff *et al.*, 1990; Scheff *et al.*, 1996). A decrease in the total number of synapses —accompanied by brain atrophy— has been also reported in CA1, the DG and some cingulate and temporal cortices (Scheff *et al.*, 2006, 2007, 2011, 2015; Montero-Crespo *et al.*, 2020*b*). However, other studies have not found differences in synaptic density in layers III and V of EC samples from AD cases (Scheff *et al.*, 1993). These discrepancies may be due to differences in the methodologies used. For example, a lower number of synapses has been described close to β-amyloid plaques (Dorostkar *et al.*, 2015; Garcia-Marin *et al.*, 2009; Blazquez-Llorca *et al.*, 2013), whereas we have examined the β-amyloid plaque-*free* neuropil. Furthermore, numerous studies have estimated the synaptic density using indirect methods — either using light microscopy to count immunoreactive puncta for synaptic markers (Honer *et al.*, 1992; Masliah *et al.*, 1990), or employing conventional transmission electron microscopy to examine single or few serial ultrathin sections (Scheff *et al.*, 1993). Quantification of synaptic density in single ultrathin sections using transmission electron microscopy to

infer 3D characteristics of synaptic junctions observed in two dimensions may lead to inaccurate synaptic density estimations (see Merchán-Pérez *et al.*, 2009). ..Thus, the present results revealing a lower number of synapses per volume of neuropil, along with the atrophy of the EC compared to controls, suggest a dramatic decrease in the absolute number of synapses in AD cases in these EC layers.

Synaptic loss has been widely reported as the characteristic that best correlates with cognitive deficit in AD patients (Arendt, 2009; Dickson *et al.*, 1995; Masliah *et al.*, 2001; Selkoe, 2002; Sze *et al.*, 1997; Terry *et al.*, 1991; reviewed in Colom-Cadena *et al.*, 2020). Synaptic loss occurs in the early stages of the disease, affecting firstly the subcortical regions and the EC, and progressing to other cortical regions (Braak and Braak, 1991; Braak and Del Tredici, 2012). Tau protein and β-amyloid peptide in pathological conditions could have toxic effects on synapses leading to synaptic loss and/or dysfunction in AD (Zhou *et al.*, 2017; reviewed in Henstridge *et al.*, 2016; Rajmohan and Reddy, 2017). This synaptic loss and impairment may cause dysfunction in the cortical circuits contributing to the decline in cognition (reviewed in Colom-Cadena *et al.*, 2020).

Interestingly, no changes in the proportions of AS and SS were observed; therefore, the lower synaptic density in AD cases might affect AS and SS equally, which is in line with our previous results in the transentorhinal cortex (Domínguez-Álvaro *et al.*, 2018). Since most of the synapses are excitatory synapses (~92% AS), it can be concluded that the decrease results in a massive loss of AS in particular.

Finally, the 3D spatial distribution of the synapses in the neuropil in all the samples fitted a random spatial distribution model. Previous studies in the plaque-free neuropil of AD cases also showed a random distribution pattern of the synapses in other brain regions from control and AD cases (Blazquez-Llorca *et al.*, 2013; Domínguez-Álvaro *et al.*, 2018; Montero-Crespo *et al.*, 2020*a, b*). Therefore, the random distribution pattern of synapses in the neuropil does not appear to be affected by the lower synaptic density in AD cases.

Shape and size of the synapses

There are very few studies on human brain at the ultrastructural level that provide 3D data on the morphological characteristics of the synaptic junctions to compare with our

findings. In the examined EC layers, excitatory AS were larger than inhibitory SS, as previously shown in human transentorhinal cortex (Domínguez-Álvaro *et al.*, 2018) and in several strata from the hippocampal CA1 (Montero-Crespo *et al.*, 2020*a*). Furthermore, no differences between layers were found regarding the SAS area of AS in AD cases (136,166 nm^2 in layer II and 122,727 nm^2 in layer III), which was in contrast with our previous results in control EC showing larger synapses in layer III (Domínguez-Álvaro *et al.*, 2020).However, the synaptic size in AD samples differs from that of control individuals, with larger and more complex synapses in layer II and a greater proportion of smaller synapses in layer III.

Several EM studies carried out with samples of human brain tissue have reported an increase in the size of synaptic apposition, and this has been suggested as a possible compensatory mechanism for the synaptic loss (reviewed in Scheff and Price, 2006). Models studying the relationship between the size of synaptic junctions and the probability of neurotransmitter release suggest that larger synapses (with a greater number of postsynaptic receptors, mainly AMPA receptors) may produce more powerful, homogeneous and numerous synaptic responses, while smaller synapses (with fewer receptors, mainly NMDA) may produce weaker and more variable responses (Montes *et al.*, 2015). Also, larger synapses have a higher number of AMPA receptors, while smaller synapses have a higher concentration of NMDA receptors (Kharazia and Weinberg, 1999). Thus, alterations in the normal size of the synaptic junction may change the proportion of postsynaptic receptors, thereby modifying the synaptic response.

Regarding synaptic shape, we found a higher proportion of horseshoe synapses in layer II from AD cases. In layer III from these AD individuals, higher proportion of AS with macular and fragmented shape were found along with a lower proportion of perforated AS synapses. Several studies have linked an increase in synaptic complexity to an increase in the efficiency of synaptic transmission, via the insertion of new receptors in the postsynaptic membrane (Lüscher *et al.*, 2000). Perforated synapses have higher immunoreactivity for glutamate receptors than non-perforated synapses (Ganeshina *et al.*, 2004*a,b*). Under normal conditions, macular synapses have the capacity to progressively increase their perimeter, adopting a more tortuous perimeter with perforations and indentations (Geinisman *et al.*, 1987; 1991; 1992*a, b*).

On the contrary, the larger proportion of macular AS in layer III (around 83% in AD cases, versus 76% in control cases) and the corresponding lower number of perforated synapses (about half the number found in control cases) supports the evidence for a larger number of simple synapses in this layer in AD cases, which is in turn supported by the finding of a higher proportion of smaller synapses described above. However, the higher proportion of fragmented AS in layer III from AD cases may indicate the above-mentioned compensatory response to the synaptic loss. Conversely, small macular synapses from layer III may be more susceptible to damage resulting in a reduction in their numbers. Fragmented synapses have been proposed to be specialized synapses that may produce a greater synaptic response compared to synapses with a single PSD (Geinisman *et al.*, 1987; 1991; 1992*a, b*; 1993; Ganeshina *et al.*, 2004*b*; Toni *et al.*, 2001). Several studies have described an increase in the number of fragmented synapses in the rat hippocampus as a result of synapse remodeling after repeated stimulation or long-term potentiation (Geinisman *et al.*, 1991; 1992*a,b*; 1993; Toni *et al.*, 2001). During this remodeling process, a synapse with a continuous disk-shaped PSD (macular) may increase its size by forming one or more holes, eventually developing a perimeter with a horseshoe shape until it finally splits into two separate PSDs (Geinisman *et al.*, 1987). Fragmented synapses could represent a final structural stage to constitute a specialized synaptic contact with unusually high synaptic efficiency. That is, synaptic morphology may be selectively altered by layer, with a non-homogenous pattern of changes, which would differentially affect the circuits in which these layers are involved.

Therefore, synaptic changes in layer II and III might be part of a remodeling process of the remaining synapses, which overcomes the overall synaptic loss. If the remodeling process involves an increase in the proportion of synapses with more complex morphology, it could be hypothesized that the morphological changes in AD would trigger compensatory mechanisms during the development of the disease. However, this type of compensatory mechanism may fail or be deficient, leading to a decline in the synaptic functionality accompanying the progression of the disease.

Postsynaptic targets

Despite the lower synaptic density in AD cases, no changes in the distribution and types of postsynaptic targets were found. In the AD samples, it was found that excitatory

axons preferentially targeted dendritic spines and inhibitory axons preferentially targeted dendritic shafts. Moreover, the most frequent combinations were axodendritic AS (established on dendritic shafts) and axospinous AS (on dendritic spine heads). These findings were similar to the results of our previous analysis in control cases in the same EC layers (Domínguez-Álvaro *et al.*, 2020) and in layer II of the TEC (Domínguez-Álvaro *et al.*, 2019). However, the analysis of postsynaptic targets in AD samples in layer II of the TEC revealed a lower number of excitatory synapses on dendritic spine heads (Domínguez-Álvaro *et al.*, 2019). Therefore, changes in the proportions of postsynaptic targets seem to be region-specific.

In addition, since the majority of the synapses that a pyramidal cell receives are on dendritic spines and they represent the vast majority of AS synapses (DeFelipe and Fariñas, 1992), the present data do not seem to be related to a loss of dendritic spines. In this regard, although the proportion of axospinous synapses in AD cases do not show differences in layers II and III of the EC compared to control, this particular type of synapse may have been altered, as suggested by the present data on size and shape modifications. Therefore, it may be that the axospinous synapses in EC from AD cases are functionally altered even though no changes were found in their proportions.

Implications of the synaptic changes

I EC provides excitatory inputs to the hippocampus: the indirect pathway (trisynaptic), from layer II neurons, and the direct pathway (monosynaptic) from layer III (reviewed in Insausti and Amaral, 2012; Marks *et al.*, 2020). Neuronal projections from both layers give rise to the perforant pathway, which has generally been reported to be weakened in AD (e.g., Hyman *et al.*, 1986). Moreover, both layers receive cortical afferents from diverse brain regions, as well as from the parahippocampal and perirhinal cortex (reviewed in Schultz *et al.*, 2015).

In layer II of the EC, there are two subpopulations of excitatory neurons: stellate neurons (which project to DG, CA3 and CA2) and pyramidal neurons (which project to *stratum lacunosum* in CA1). These projections, constituting the trisynaptic pathway, seem to be related to contextual memories (reviewed in Mark *et al.*, 2020). It has been proposed that this pathway is more susceptible to premature degeneration than the monosynaptic pathway (Van Hoesen *et al.*, 2006; Llorens-Martín *et al.*, 2014). In addition, pyramidal neurons from EC layer III directly project to pyramidal neuron

dendrites located in the *stratum molecular*e of CA1, and it has been proposed that these monosynaptic excitatory inputs drive temporal association learning (reviewed in Mark *et al.*, 2020).

The present study suggests a lower number of synapses per volume, as well as morphological synaptic alterations in the EC from AD cases in layers II and III. Since the AD cases examined in the present study correspond to advanced stages of the disease, we do not know *when* the synaptic alterations occurred. Considering that there is neuronal loss, the lower number of synapses may be explained —at least in part— by the loss of local axons of these neurons, at least at the earlier stages of the disease. However, the lower number of synapses may also be explained by a loss of long-distance axonal projections from neurons that die in distant cortical regions that are also affected by the disease.

Interindividual variability

AD cases showed clear interindividual variability in the synaptic density (Supplementary Fig. 2; Supplementary Table 4). Technical effects could be ruled out given that the postmortem delays were all similar and the procedures used were the same. Moreover, all of the AD cases examined were women aged between 80 and 86 years old; therefore, variability due to sex and aging could also be ruled out.

Considering the above-mentioned toxic effect of tau protein and β-amyloid peptide on the synapses, a relationship between the degree of disease progression and the synaptic loss might be expected: the greater the degree of the pathology, the greater the synaptic loss. Subject VK16, who presented a high score for neuropathology and disease progression (Braak/CERAD: VI/C), also had the lowest synaptic density in both layers (0.12 synapse/μm^3; Supplementary Fig. 2; Supplementary Table 4). However, subject VK22, who also had a high score for neuropathology and disease progression (V/C), had a synaptic density of more than double (0.29 and 0.27 synapse/μm^3, for layers II and III, respectively) and both cases, VK16 and VK22, suffered dementia. However, subject IF1 did not present evidence of dementia despite the fact that this subject had a high level of pathology (IV/B) and low synaptic density, which was similar to VK22 (0.21 and 0.27 synapse/μm^3, for layers II and III, respectively). However, the cortical thickness of case IF1 was 2.3 mm, whereas —in VK16 and VK22— the cortical layers were thinner (1.19 and 1.51 mm, respectively; Supplementary Table 1). As pointed out

by Ferrer (2012), it should be kept in mind that AD —at least and limited to the entorhinal and transentorhinal cortices (stages I–II)— affects about 80% of individuals over 65 years, but dementia only occurs in a small percentage of individuals in this age bracket (the prevalence of dementia in AD increases to 25% in 80-year-old individuals). Thus, it is possible that this particular case (IF1) may represent a pre-dementia stage of AD (prodromal AD).

Finally, comparison between control and AD cases in the present study should be interpreted with caution since the control group was made up of men aged 40 to 66 years old, whereas the AD cases were women aged 80 to 88 years old. Although no sex-based differences have been reported with aging in the human cerebral cortex (Scheff *et al.*, 2001), previous studies on synaptic density in the human *temporal* cortex have shown differences depending on the sex (Alonso-Nanclares *et al.*, 2008). Nevertheless, no similar EM studies have been performed in the EC in individuals with different ages and sexes. Thus, the lower synaptic density found in AD cases might also be the results of sex or age effects. Further studies using human brain tissue from older control cases would be necessary to determine whether or not these differences in the synaptic density are due to these factors, as opposed to the AD *per se*. Nevertheless, it is important to point out that only the neuropil without plaques was examined in the present study, whereas it is well established that the neuropil which is adjacent to —and is surrounding— the plaques shows synaptic alterations (Blazquez-Llorca *et al.*, 2013). Thus, it is possible that the neuropil lacking plaques in AD cases displays "normal" characteristics, and differences observed in our study comparing to the control group might be due to factors related to sex and age.

Conclusions

In the present study, we found, in addition to synaptic loss, changes in the morphology of the synapses in AD compared to control cases. These structural changes may contribute to the anatomical basis for the impairment of cognitive functions in AD. Despite the large number of synapses analyzed (5000 synapses), and the proven robustness of the methodology used in this study, it should be kept in mind that (i) the data comes from the analysis of 4 control cases and 4 AD cases and (ii) we cannot rule out sex- and age-related factors that may influence the differences observed between the two groups. In order to address these remaining issues, it would be necessary to

perform further studies using FIB/SEM or other similar techniques to reconstruct thousands of synapses in aged control cases of both sexes.

Materials and Methods

Tissue preparation

Human brain samples were obtained following the guidelines of the Institutional Ethical Committee (Table 4). See further details in Supplementary Materials and Methods, for *Tissue preparation.*

Sections containing EC were selected for Nissl staining, immunohistochemistry and electron microscopy processing (Fig. 3), as described in Supplementary Materials and Methods, for *Immunohistochemistry* and *Tissue processing for Electron Microscopy.*

Cortical thickness estimation

In order to estimate the atrophy of the EC, we measured the cortical thickness in three to five toluidine blue-stained semithin sections from each of the cases, obtained in the coronal plane of the cortex and containing the entire cortex, from the pial surface to the white matter. Measurements of the distance between the pial surface and the boundary with the white matter were performed using Fiji program (ImageJ 1.51; NIH, USA; http://imagej.nih.gov/ij/). To average data, three measurements were made per section.

Volume fraction estimation of cortical elements

Three to five semithin sections (1–2µm thick) stained with 1% toluidine blue were used to estimate the respective volume fractions (Vv) occupied by blood vessels, cell bodies (glia and neurons) and neuropil. This estimation was performed applying the Cavalieri principle (Gundersen *et al.*, 1988) by point counting using the integrated Stereo Investigator stereological package (Version 8.0, MicroBrightField Inc., VT, USA) attached to an Olympus light microscope (Olympus, Bellerup, Denmark) at 40x magnification. A grid, whose points covered an area of 400µm^2, was overlaid over each semithin section to determine the V_v occupied by the different elements: neurons, glia, blood vessels and neuropil.

Three-dimensional electron microscopy

The araldite block containing the tissue was used to obtain images stacks from the EC (Fig. 4) using a dual beam microscope (FIB/SEM; Crossbeam® 540 electron

microscope, Carl Zeiss NTS GmbH, Oberkochen, Germany). See further details in Supplementary Materials and Methods, *Three-dimensional electron microscopy.*

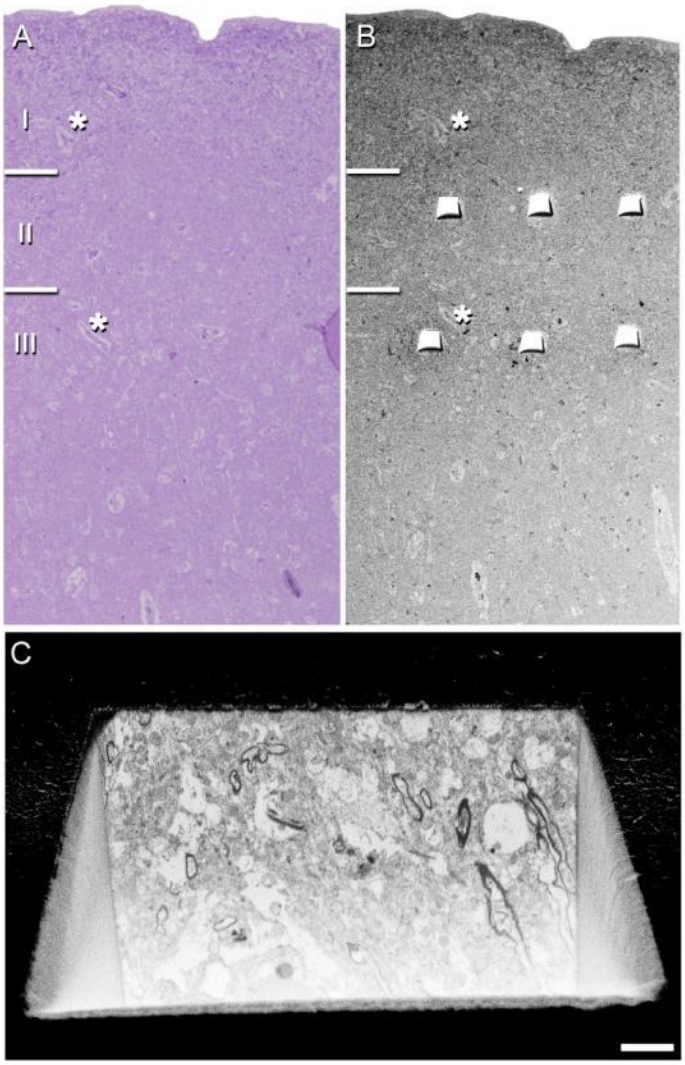

Figure 4. Correlative light/electron microscopy of layer II and III of the EC. Delimitation of layers is based on the staining pattern of 1 µm-thick semithin section, stained with toluidine blue **(A)**, which is adjacent to the block for FIB/SEM imaging **(B)**. **(B)** SEM image illustrating the block surface with trenches made in the neuropil (three per layer). Asterisks in A and B point to the same blood vessels, showing that the exact location of the region of interest was accurately determined. **(C)** SEM image showing the front of a trench made to expose the tissue and to acquire the FIB/SEM stack of images at the final magnification. Scale bar (in C): 70µm in A; 85µm in B; 3µm in C.

In total, 24 stacks of images of the neuropil from layer II and III of the EC from AD cases were obtained (three stacks for each of the 4 cases, with a total volume studied of 9,006 μm^3, Table 1). The data obtained from these stacks of images were compared to the data obtained in the same regions of four control cases, previously described by Domínguez-Álvaro *et al.* (2020).

Synaptic three-dimensional analysis

FIB/SEM stacks of images were analyzed using EspINA software (*EspINA Interactive Neuron Analyzer*, 2.1.9; https://cajalbbp.es/espina/), which allows the segmentation of synapses in the reconstructed 3D volume (Morales *et al.*, 2011; Supplementary Fig. 7). Since the EspINA software allows navigation through the stack of images (Fig. 5; Supplementary Fig. 7), it was possible to unambiguously identify every synapse as asymmetric synapses (AS) or symmetric synapses (SS), based on the thickness of the PSD (Fig. 5). EspINA also allowed the application of an unbiased 3D counting frame (CF) to obtain the synaptic density per volume (for details, see Merchán-Pérez *et al.*, 2009). Geometrical characteristics —such as size— and spatial distribution features (centroids) of each reconstructed synapse were also calculated by EspINA. See further details in Supplementary Materials and Methods, *Synaptic three-dimensional analysis*.

In addition, the visualization of each 3D reconstructed synapse allowed us to determine the synaptic morphology. Based on the presence of perforations or indentations in their perimeters, the synapses could be classified into four types (Fig.1A): macular (with a flat, disk-shaped PSD), perforated (with one or more holes in the PSD), horseshoe (with an indentation in the perimeter of the PSD) or fragmented (with two or more physically discontinuous PSDs) (for a detailed description, see Domínguez-Álvaro *et al.*, 2019; Santuy *et al.*, 2018).

To identify the postsynaptic targets of the synapses, we navigated the image stack using EspINA to determine whether the postsynaptic element was a dendritic spine ('spine' or 'spines', for simplicity) or a dendritic shaft. See further details in Supplementary Materials and Methods, *Synaptic three-dimensional analysis*.

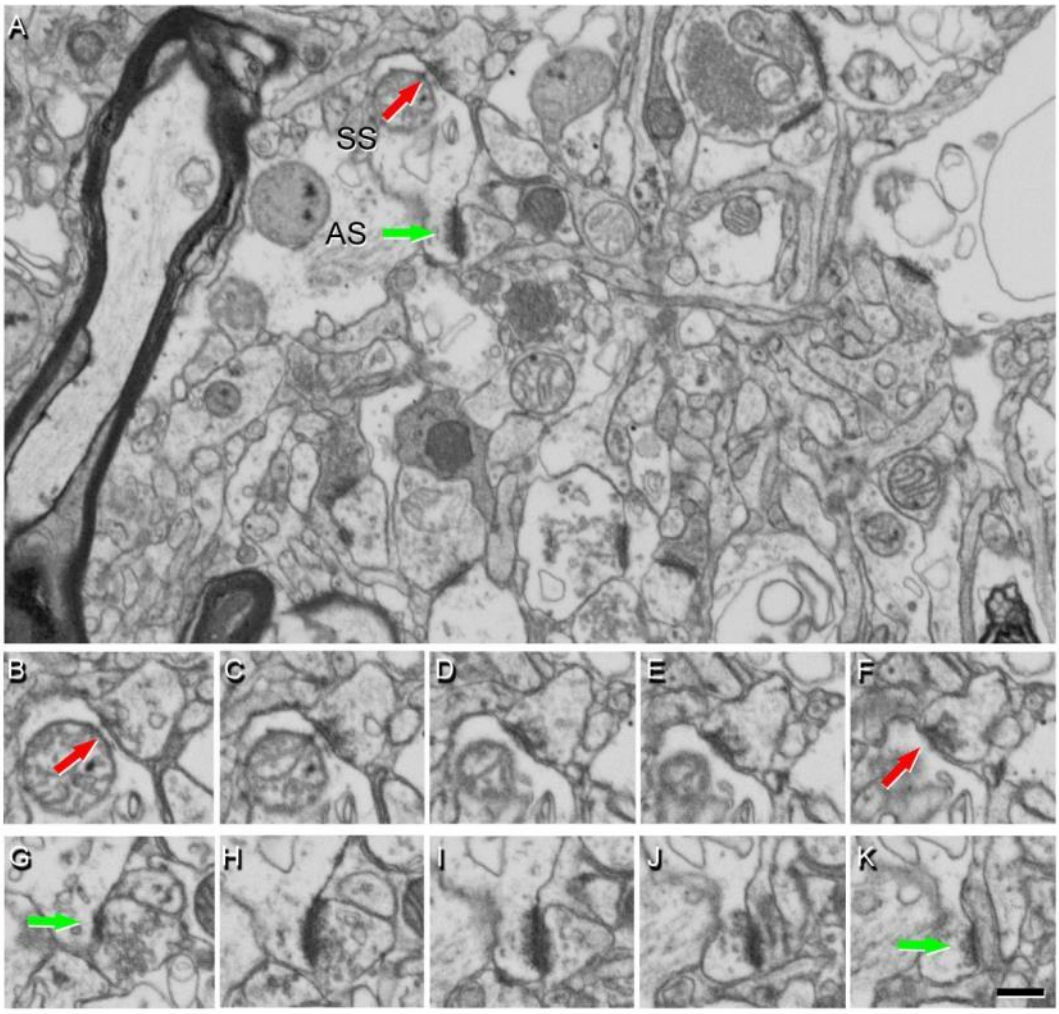

Figure 5. Identification of synapses in serial electron microscopy images obtained by FIB/SEM. (A) Image from layer II showing the neuropil from an AD case, with two synapses indicated (arrows) as examples of asymmetric (AS, green) and symmetric synapses (SS, red). Synapse classification was based on examination of the full sequence of serial images; an SS can be visualized in **B–F**, and an AS in **G–K**. Scale bar (in K): 1,000 nm in A; 1,300 nm in B–K.

Spatial Distribution Analysis of Synapses

To analyze the spatial distribution of synapses, spatial point-pattern analysis was performed as described elsewhere (Merchán-Pérez *et al.*, 2014). For each of the 24 different samples, we calculated three functions commonly used for spatial point pattern analysis: F, G and K functions (for a detailed description, see Blazquez-Llorca *et al.*, 2015). Additionally, we measured the distance of each synapse to its nearest synapse, to

compare control and AD samples. This study was carried out using the Spatstat package and R Project program (Baddeley *et al.*, 2015).

Statistical analysis

To determine possible differences between the control and AD samples, statistical comparisons of the following parameters were carried out using the unpaired Mann-Whitney (MW) nonparametric U-test: cortical thickness; synaptic density; type of synapse (AS or SS); SAS size; synaptic shape; postsynaptic targets; and distance to the nearest neighboring synapse. To determine possible differences between control and AD samples regarding volume fractions (neuronal and glial cell bodies, blood vessels and neuropil), parametric t-test were carried out. Frequency distribution analyses were performed using Kolmogorov-Smirnov (KS) nonparametric test.

To perform statistical comparisons of AS and SS proportions, chi-square (χ^2) test was used for contingency tables. The same method was used to study whether there were significant differences between groups in relation to the shape of the synaptic junctions and their postsynaptic target. See further details in Supplementary Materials and Methods.

Statistical analyses were performed using the GraphPad Prism statistical package (Prism 8.4.2 for Windows, GraphPad Software Inc., USA) and SPSS (IBM SPSS Statistics v24, IBM Corp., Armonk, NY, USA).

Data availability

Most data is available in the main text and the supplementary tables. The datasets used and analyzed are also available from the corresponding author on reasonable request, and control datasets are published on the EBRAINS Knowledge Graph (DOI: 10.25493/3GMJ-FEZ).

Acknowledgments

We would like to thank Carmen Álvarez and Lorena Valdés for their technical assistance, and Nick Guthrie for his excellent text editing.

Funding

This study was funded by grants from the following entities: Spanish "Ministerio de Ciencia e Innovación" grant PGC2018-094307-B-I00; the Cajal Blue Brain Project (the Spanish partner of the Blue Brain Project initiative from EPFL, [Switzerland]); Centro de Investigación Biomédica en Red sobre Enfermedades Neurodegenerativas (CIBERNED, Spain, CB06/05/0066); the Alzheimer's Association (ZEN-15-321663); the European Union's Horizon 2020 Framework Programme for Research and Innovation under grant agreement No. 945539 (Human Brain Project SGA3). MM-C was awarded a research fellowship from the Spanish "Ministerio de Educación y Formación Profesional" (FPU14/02245) and LB-L gained a postdoctoral contract from the UNED (Plan de Promoción de la Investigación, 2014-040-UNED-POST).

Competing interest

The authors declare that they have no competing interests.

Ethics approval

Human brain samples were obtained with informed consent, following the guidelines of the ethics committees of the institutions involved. The consent of the patients was obtained and the sampling procedure was approved by the Institutional Ethics Committees of the Albacete University Hospital (Albacete, Spain), Bellvitge University Hospital (Barcelona, Spain) and *Centro Alzheimer Fundación Reina Sofía*, CIEN Foundation (Madrid, Spain). The tissue was obtained following national laws and international ethical and technical guidelines on the use of human samples for biomedical research purposes. Tissue from these human brain samples has been used in previous studies (Domínguez-Álvaro *et al.*, 2018, 2019, 2020; Montero-Crespo *et al.*, 2020)

Authors' contributions

M D-A, Conceptualization, Data curation, Software, Formal analysis, Investigation, Methodology, Writing - review and editing; M M-C, Data curation, Software, Methodology; L B-L, Conceptualization, Supervision, Validation, Methodology, Writing - review and editing; J DeF, Conceptualization, Resources, Supervision, Funding acquisition, Validation, Project administration, Writing – review and editing; L A-N, Conceptualization, Data curation, Formal analysis, Supervision, Validation, Investigation, Methodology, Writing - original draft, Writing - review and editing.

References

1. Alonso-Nanclares L, Gonzalez-Soriano J, Rodríguez JR, DeFelipe J. Gender differences in human cortical synaptic density. Proc Natl Acad Sci USA 2008; 105: 14615–14619.
2. Alzheimer's Association. Alzheimer's disease facts and figures. Alzheimer Dement 2020; 16: 391.
3. Andrade-Moraes CH, Oliveira-Pinto AV, Castro- Fonseca E, da Silva CG, Guimarães DM, Szczupak D *et al.* Cell number changes in Alzheimer's disease relate to dementia, not to plaques and tangles. Brain 2013; 136: 3738-52.
4. Arendt T. Synaptic degeneration in AD. Acta Neuropathol 2009; 118:167–179.
5. Baddeley A, Rubak E, Turner R. Spatial point patterns: methodology and applications with R. Boca Raton (CA): Chapman and Hall/ CRC Press; 2015.
6. Blazquez-Llorca L, Merchán-Pérez Á, Rodríguez JR, Gascón J, DeFelipe J. FIB/SEM technology and AD: three-dimensional analysis of human cortical synapses. J Alzheimers Dis 2013; 34:995–1013.
7. Blazquez-Llorca L, Woodruff A, Inan M, Anderson SA, Yuste R, DeFelipe J, Merchán-Pérez Á. Spatial distribution of neurons innervated by chandelier cells. Brain Struct Funct 2015; 220:2817–2834.
8. Braak H, Braak E. Neuropathological stageing of Alzheimer-related changes. Acta Neuropathol 1991; 82: 239-259.
9. Braak H, Del Tredici K. Where, when, and in what form does sporadic Alzheimer's disease begin? Curr Opin Neurol 2012; 25:708–714.

10. Braak H, Del Tredici K. From the Entorhinal Region via the Prosubiculum to the Dentate Fascia: Alzheimer Disease-Related Neurofibrillary Changes in the Temporal Allocortex. J Neuropathol Exp Neurol 2020; 79: 163-175.
11. Chen Y, Fu AKY, Ip NY. Synaptic dysfunction in Alzheimer's disease: Mechanisms and therapeutic strategies. Pharmacol Ther 2019; 195: 186-198.
12. Coleman P, Federoff H, Kurlan R. A focus on the synapse for neuroprotection in Alzheimer disease and other dementias. Neurology 2004; 63:1155–1162.
13. Colom-Cadena M, Spires-Jones T, Zetterberg H, Blennow K, Caggiano A, DeKosky ST, et al() The Clinical Promise of Biomarkers of Synapse Damage or Loss in Alzheimer's Disease. Alzheimers Res Ther 2020; 12:21.
14. DeFelipe J, Fairén A. A simple and reliable method for correlative light and electron microscopic studies. J Histochem Cytochem 1993; 41:769–772.
15. DeFelipe J, Fariñas I. The pyramidal neuron of the cerebral cortex: morphological and chemical characteristics of the synaptic input. Prog Neurobiol 1992; 39: 563–607.
16. Dickson DW. The Pathogenesis of Senile Plaques. J Neuropathol Exp Neurol 1997; 56: 321-39.
17. Dickson DW, Crystal HA, Bevona C, Honer W, Vincent I, Davies P. Correlations of synaptic and pathological markers with cognition of the elderly. Neurobiol Aging 1995; 16: 285-304.
18. Domínguez-Álvaro M, Montero-Crespo M, Blazquez-Llorca L, Insausti R, DeFelipe J, Alonso-Nanclares L. Three-dimensional analysis of synapses in the transentorhinal cortex of Alzheimer’s disease patients. Acta Neuropathol Commun 2018; 6: 20.
19. Domínguez-Álvaro M, Montero-Crespo M, Blazquez-Llorca L, DeFelipe J, Alonso-Nanclares L. 3D Electron Microscopy Study of Synaptic Organization of the Normal Human Transentorhinal Cortex and Its Possible Alterations in Alzheimer's Disease. eNeuro 2019; 6:1-17.
20. Domínguez-Álvaro M, Montero-Crespo M, Blazquez-Llorca L, DeFelipe J, Alonso-Nanclares L. 3D ultrastructural study of synapses in the human entorhinal cortex. Cerebral Cortex 2020; 10.1093/cercor/bhaa233.
21. Dorostkar MM, Zou C, Blazquez-Llorca L, Herms J. Analyzing dendritic spine pathology in AD: problems and opportunities. Acta Neuropathol 2015; 130:1–19.

22. Fakhoury M. Microglia and Astrocytes in Alzheimer's Disease: Implications for Therapy. Curr Neuropharmacol 2018; 16: 508–518.
23. Ferrer I. Defining Alzheimer as a common age-related neurodegenerative process not inevitably leading to dementia. Prog Neurobiol 2012; 97: 38–51.
24. Forner S, Baglietto-Vargas D, Martini AC, Trujillo-Estrada L, LaFerla FM. Synaptic Impairment in Alzheimer's Disease: A Dysregulated Symphony. Trends Neurosci 2017; 40: 347-357.
25. Ganeshina O, Berry RW, Petralia RS, Nicholson DA, Geinisman Y. Differences in the expression of AMPA and NMDA receptors between axospinous perforated and nonperforated synapses are related to the configuration and size of postsynaptic densities. J Comp Neurol 2004a; 468: 86–95.
26. Ganeshina O, Berry RW, Petralia RS, Nicholson DA, Geinisman Y. Synapses with a segmented, completely partitioned postsynaptic density express more AMPA receptors than other axospinous synaptic junctions. Neuroscience 2004b; 125: 615–623.
27. Garcia-Marin V, Blazquez-Llorca L, Rodriguez JR, Boluda S, Muntane G, Ferrer I, DeFelipe J. Diminished perisomatic GABAergic terminals on cortical neurons adjacent to amyloid plaques. Front Neuroanat 2009; 3:28.
28. Geinisman Y, Morrell F, DeToledo-Morrell L. Axospinous synapses with segmented postsynaptic densities: a morphologically distinct synaptic subtype contributing to the number of profiles of 'perforated' synapses visualized in random sections. Brain Res 1987; 423: 179–188.
29. Geinisman Y, DeToledo-Morrell L, Morrell F. Induction of long-term potentiation is associated with an increase in the number of axospinous synapses with segmented postsynaptic densities. Brain Res 1991; 566: 77–88.
30. Geinisman Y, DeToledo-Morrell L, Morrell F, Persina IS, Rossi M. Structural synaptic plasticity associated with the induction of long-term potentiation is preserved in the dentate gyrus of aged rats. Hippocampus 1992a; 2: 445–456.
31. Geinisman Y, Morrell F, DeToledo-Morrell L. Increase in the number of axospinous synapses with segmented postsynaptic densities following hippocampal kindling. Brain Res 1992b; 569: 341–347.
32. Geinisman Y, DeToledo-Morrell L, Morrell F, Heller RE, Rossi M, Parshall RF. Structural synaptic correlate of longterm potentiation: Formation of axospinous

synapses with multiple, completely partitioned transmission zones. Hippocampus 1993; 3: 435-446.

33. Gomez-Isla T, Price JL, McKeel DW, Morris JC, Growdon JH, Hyman BT. Profound Loss of Layer II Entorhinal Cortex Neurons Occurs in Very Mild Alzheimer's Disease. J Neurosci 1996; 16:4491-4500.
34. Gundersen HJG, Bendtsen TF, Korbo L, Marcussen N, Miziller A, Nielsen K, *et al.* Some new, simple and efficient stereological methods and their use in pathological research and diagnosis. APMIS 1988; 96:379–394.
35. Gunten A, Kövari E, Bussière T, Rivara CB, Gold G, Bouras C *et al.* Cognitive impact of neuronal pathology in the entorhinal cortex and CA1 field in Alzheimer's disease. Neurobiol Aging 2006; 27: 270-277.
36. Henstridge CM, Pickett E, Spires-Jones TL. Synaptic pathology: a shared mechanism in neurological disease. Ageing Res Rev 2016; 28:72–84.
37. Honer WG, Dickson DW, Gleeson J, Davies P. Regional synaptic pathology in AD. Neurobiol Aging 1992; 13: 375-382.
38. Hyman BT, Van Hoesen GW, Kromer LJ, Damasio AR. Perforant pathway changes and the memory impairment of Alzheimer's disease. Ann Neurol 1986; 20: 472-81.
39. Insausti R, Amaral DG. Hippocampal Formation. In: Mai JK, Paxinos G, eds. The Human Nervous System. Cambridge (MA): Academic Press; 2012. p. 896-942.
40. Kharazia VN, Weinberg RJ. Immunogold localization of AMPA and NMDA receptors in somatic sensory cortex of albino rat. J Comp Neurol 1999; 412: 292–302.
41. Kondo H, Lavenex P, Amaral DG. Intrinsic connections of the macaque monkey hippocampal formation: II. CA3 connections. J Comp Neurol 2009; 515:349-377.
42. Lavenex P, Amaral DG. Hippocampal-neocortical interaction: a hierarchy of associativity. Hippocampus 2000; 10:420-430.
43. Llorens-Martín M, Blazquez-Llorca L, Benavides-Piccione R, Rábano A, Hernandez F, Avila J *et al.* Selective alterations of neurons and circuits related to early memory loss in AD. Front Neuroanat 2014; 8:38.
44. Lüscher C, Nicoll RA, Malenka RC, Muller D. Synaptic plasticity and dynamic modulation of the postsynaptic. Nat Neurosci 2000; 3: 545–550.

45. Marks WD, Yamamoto N, Kitamura T. Complementary roles of differential medial entorhinal cortex inputs to the hippocampus for the formation and integration of temporal and contextual memory. Eur J Neurosci 2020; 00: 1-18.
46. Masliah E, Terry RD, Alford M, Deteresa R. Quantitative Immunohistochemistry of Synaptophysin in Human Neocortex: An Alternative Method to Estimate Density of Presynaptic Terminals in Paraffin Sections. J Histochem Cytochem 1990; 38: 837–844.
47. Merchán-Pérez A, Rodríguez JR, Alonso-Nanclares L, Schertel A, DeFelipe J. Counting synapses using FIB/SEM microscopy: a true revolution for ultrastructural volume reconstruction. Front Neuroanat 2009; 3:18.
48. Merchán-Pérez A, Rodríguez JR, González S, Robles V, DeFelipe J, Larrañaga P, Bielza C. Three-dimensional spatial distribution of synapses in the neocortex: a dual-beam electron microscopy study. Cereb Cortex 2014; 24:1579–1588.
49. Mirra SS, Heyman A, McKeel D, Sumi SM, Crain BJ, Brownlee LM et al. The consortium to establish a registry for AD (CERAD). Part II. Standarization of the neuropathologic assessment of AD. Neurology 1991; 41:479–486.
50. Montero-Crespo M, Domínguez-Álvaro M, Rondón-Carrillo P, Alonso-Nanclares L, DeFelipe J, Blazquez-Llorca L. Three-dimensional synaptic organization of the human hippocampal CA1 field. eLife 2020a; 9:e57013.
51. Montero-Crespo M, Domínguez-Álvaro M, Alonso-Nanclares L, DeFelipe J, Blazquez-Llorca L. 3D analysis of synaptic organization in the hippocampal CA1 region in Alzheimer´s disease. Brain 2020b (in press).
52. Montes J, Peña JM, DeFelipe J, Herreras O, Merchan-Perez A. The influence of synaptic size on AMPA receptor activation: a Monte Carlo model. PLoS One 2015; 10: e0130924.
53. Morales J, Alonso-Nanclares L, Rodríguez JR, DeFelipe J, Rodríguez Á, Merchán-Pérez Á. Espina: a tool for the automated segmentation and counting of synapses in large stacks of electron microscopy images. Front Neuroanat 2011; 18:18.
54. Muramori, F., Kobayashi, K., and Nakamura, I. A quantitative study of neurofibrillary tangles, senile plaques and astrocytes in the hippocampal subdivisions and entorhinal cortex in Alzheimer's disease, normal controls and non-Alzheimer neuropsychiatric diseases. Psychiatry Clin Neurosci 1998; 52, 593–599.

55. Peters A, Palay SL. The morphology of synapses. J Neurocytol 1996; 25:687–700.
56. Rajmohan R, Reddy PH. Amyloid-Beta and Phosphorylated tau accumulations cause abnormalities at synapses of AD neurons. J Alzheimers Dis 2017; 57:975–999.
57. Santuy A, Rodríguez J, DeFelipe J, Merchán-Pérez A. Study of the Size and Shape of Synapses in the Juvenile Rat Somatosensory Cortex with 3D Electron Microscopy. eNeuro 2018; 5:1-14.
58. Scheff SW, Price DA. Synapse loss in the temporal lobe in AD. Ann Neurol 1993; 33:190–199.
59. Scheff SW, Price DA. Synaptic density in the inner molecular layer of the hippocampal dental gyrus in Alzheimer's disease. J Neuropathol Exp Neurol 1998; 57:1146–1153.
60. Scheff SW, Price DA. Synaptic pathology in AD: a review of ultrastructural studies. Neurobiol Aging 2003; 24:1029–1046.
61. Scheff SW, Price DA. AD-related alterations in synaptic density: neocortex and hippocampus. J Alzheimers Dis 2006; 9:101–115.
62. Scheff SW, Dekosky ST, Price DA. Quantitative assessment of cortical synaptic density in Alzheimer's disease. Neurobiol Aging 1990; 11:29–37.
63. Scheff SW, Sparks DL, Price DA. Quantitative assessment of synaptic density in the entorhinal cortex in Alzheimer's disease. Ann Neurol 1993; 34:356–361.
64. Scheff SW, Sparks DL, Price DA. Quantitave assessment of synaptic density in the outer molecular layer of the hippocampal dentate gyrus in Alzheimer's disease. Dementia 1996; 7:226–232.
65. Scheff SW, Price DA, Sparks LD. Quantitative assessment of possible age-related change in synaptic numbers in the human frontal cortex. Neurobiol Aging 2001; 22:355–365.
66. Scheff SW, Price DA, Schmitt FA, Mufson EJ. Hippocampal synaptic loss in early AD and mild cognitive impairment. Neurobiol Aging 2006; 27:1372–1384.
67. Scheff SW, Price DA, Schmitt FA, Dekosky ST, Mufson EJ. Synaptic alterations in CA1 in mild Alzheimer disease and mild cognitive impairment. Neurology 2007; 68:1501–1508.

68. Scheff SW, Price DA, Schmitt FA, Scheff MA, Mufson EJ. Synaptic loss in the inferior temporal gyrus in mild cognitive impairment and Alzheimer disease. J Alzheimers Dis 2011; 24:547–557.
69. Scheff SW, Price DA, Ansari MA, Roberts KN, Schmitt FA, Ikonomovic MD *et al.* Synaptic change in the posterior cingulate gyrus in the progression of AD. J Alzheimers Dis 2015; 43:1073–1090.
70. Schultz H, Sommer T, Peters J. The Role of the Human Entorhinal Cortex in a Representational Account of Memory. Front Hum Neurosci 2015; 9: 628.
71. Selkoe DJ. AD Is a Synaptic Failure. Science 2002; 298: 789-791.
72. Šimić G, Leko MB, Wray S, Harrington CR, Delalle I, Jovanov-Miloševic N *et al.* Monoaminergic neuropathology in Alzheimer's disease. Prog Neurobiol 2017; 151:101–138.
73. Solodkin A, Van Hoesen GW. Entorhinal cortex modules of the human brain. J Comp Neurol 1996; 365:610-7.
74. Sze CI, Troncoso JC, Kawas C, Mouton P, Price DL, Martin LJ. Loss of the presynaptic vesicle protein synaptophysin in hippocampus correlates with cognitive decline in Alzheimer disease. JNeuropathol Exp Neurol 1997; 56: 933-944.
75. Terry RD, Masliah E, Salmon DP, Butters N, DeTeresa R, Hill R *et al.* Physical Basis of Cognitive Alterations in Alzheimer's Disease: Synapse Loss Is the Major Correlate of Cognitive Impairment. Ann Neurol 1991; 30: 572-580.
76. Thal DR, Rüb U, Orantes M, Braak H. Phases of Aβ-deposition in the human brain and its relevance for the development of AD. Neurology 2002; 58: 1791-1800.
77. Toni N, Buchs P, Nikonenko I, Povilaitite P, Parisi L, Muller D (2001) Remodeling of synaptic membranes after induction of long-term potentiation. J Neurosci 2001; 21: 6245–6251.
78. Van Hoesen GW, Hyman BT. Hippocampal formation: anatomy and the patterns of pathology in Alzheimer´s disease. Prog Brain Res 1990; 83: 445-57.
79. Van Hoesen GW, Hyman BT, Damasio AR. Entorhinal cortex pathology in AD. Hippocampus 1991; 1:1–8.
80. Van Hoesen GW, Augustinack JC, Dierking J, Redman SJ, Thangavel R. The Parahippocampal Gyrus in Alzheimer's Disease: Clinical and Preclinical Neuroanatomical Correlates. Ann NY Acad Sci 2006; 911: 254–274.

81. Zhou L, McInnes J, Wierda K, Holt M, Herrmann AG, Jackson RJ *et al.* Tau association with synaptic vesicles causes presynaptic dysfunction. Nat Commun 2017; 8:15295.

EC layer	Group	No. AS	No. SS	No. all synapses	% AS (mean ± SD)	% SS (mean ± SD)	CF volume (μm^3)	No. AS/μm^3 (mean ± SD)	No. AS/μm^3 (mean ± SD)	No. all synapses/μm^3 (mean ± SD)	Distance to nearest neighbor (nm; mean± SD)
II	**Control**	1,553	137	1,690	91.90±2.62	8.10±2.62	4,221 (5,445)	0.37±0.05	0.03±0.01	0.40±0.03	811±33
	Alzheimer	954	90	1,044	90.53±4.27	9.47±4.27	4,409 (5,742)	0.21±0.09	0.02±0.01	0.24±0.09	906±109
III	**Control**	1,747	130	1,877	92.84±1.97	7.16±1.978	4,371 (5,466)	0.40±0.09	0.03±0.01	0.43±0.01	823±41
	Alzheimer	973	92	1,065	92.12±5.70	7.88±5.70	4,597 (5,653)	0.22±0.06	0.02±0.02	0.24±0.08	970±206

Table 1. Accumulated data obtained from the ultrastructural analysis of the neuropil from layers II and III of the EC. All volume data are corrected for shrinkage factor. Data in parentheses are not corrected with the shrinkage and the fixation artifact factors. AS: asymmetric synapses; CF: counting frame; EC: entorhinal cortex; SD: standard deviation; SS: symmetric synapses. The data for individual cases are shown in Supplementary Table 4.

EC layer	Group	Type of synapse (no. of synapses)	Area of SAS	Perimeter of SAS
II	Control	AS (1552)	110,311 ±3,229 (102,865)	1,631 ±47 (1,575)
		SS (139)	65,997 ±6,041 (61,543)	1,404 ±73 (1,356)
	Alzheimer	AS (952)	136,166 ±10,773 (126,976)	1,819 ±52 (1,757)
		SS (90)	59,232 ±6,589 (55,234)	1,239 ±72 (1,196)
III	Control	AS (1746)	124,183 ±3,265 (115,801)	1,826 ±67 (1,763)
		SS (129)	67,445 ±3,243 (62,893)	1,399 ±75 (1,351)
	Alzheimer	AS (973)	122,727 ±10,453 (114,444)	1,720 ±116 (1,661)
		SS (94)	57,271 ±14,132 (56,082)	1,343 ±272 (1,348)

Table 2. Area (mean ± sem, in nm^2) and perimeter (mean ± sem, in nm) of the SAS in layers II and III of the EC. Data on area and perimeter are corrected for shrinkage factor (Data in parentheses are not corrected with the shrinkage and the fixation artifact factors). AS: asymmetric synapses; EC: entorhinal cortex; SAS: synaptic apposition surface; sem: standard error of the mean; SS: symmetric synapses. The data for individual cases are shown in Supplementary Table 5.

EC layer	Group	Type of synapse	Macular synapses	Perforated synapses	Horseshoe synapses	Fragmented synapses	Total synapses
II	Control	AS	83.0% (1,285)	12.9% (200)	3.3% (51)	0.8% (13)	100% (1,549)
		SS	73.0% (100)	11.0% (15)	15.3% (21)	0.7% (1)	100% (137)
	Alzheimer	AS	80.6% (769)	13.4% (128)	4.9% (47)	1.1% (10)	100% (954)
		SS	73.4% (66)	12.2% (11)	12.2% (11)	2.2% (2)	100% (90)
III	Control	AS	75.9% (1,326)	19.9% (347)	3.3% (58)	0.9% (15)	100% (1,746)
		SS	65.9% (85)	15.5% (20)	17.0% (22)	1.6% (2)	100% (129)
	Alzheimer	AS	82.8% (806)	10.2% (99)	4.3% (42)	2.7% (26)	100% (973)
		SS	73.9% (68)	8.7% (8)	10.9% (10)	6.5% (6)	100% (92)

Table 3. Proportion of the different synaptic shapes in layers II and III of the EC. Data are given as percentages with the absolute number of synapses studied in parentheses. AS: asymmetric synapses; EC: entorhinal cortex; SS: symmetric synapses. Data for individual cases are shown in Supplementary Tables 6 and 7.

Patient	Sex	Age (years)	Cause of death	Postmortem delay (h)	Braak Stage	CERAD Stage	Neuropsychological diagnosis
AB1	Male	45	Lung cancer	<1	0	0	No recorded neurological alterations
AB3	Male	53	Bladder carcinoma	3.5	0	0	No recorded neurological alterations
IF10	Male	66	Bronchopneumonia and cardiac failure	2	0	0	No recorded neurological alterations
M16	Male	40	Traffic accident	3	0	0	No recorded neurological alterations
IF1	Female	80	-	2	IV	B	No evidence of cognitive impairment and dementia
VK11	Female	87	Respiratory inflammation	1.5	III–IV	A	Dementia
VK16	Female	88	-	2.5	VI	C	Dementia
VK22	Female	86	-	2	V	C	Dementia

Table 4. Clinical and neuropathological information. Braak Stages (Braak and Braak, 1991): III (NFTs —neurofibrillary tangles— in entorhinal cortex and closely related areas); III–IV (NFTs abundant in amygdala and hippocampus. Extending slightly into association cortex); V–VI (NFTs widely distributed throughout the neocortex and ultimately involving primary motor and sensory areas). CERAD Stages (Mirra et al., 1991): A (Low density of neuritic plaques); B (Intermediate density of neuritic plaques); C (High density of neuritic plaques). -: Not available.

Figure legends

Figure 1. Entorhinal cortex of control and AD cases. (Top) Plots of the medial structures including the hippocampal formation and EC from control (left) and AD (right) cases to illustrate the atrophy that occurs in AD. Plots are based on Nissl-stained coronal sections from cases AB3 and IF1. **(A–I)** Microphotographs showing the EC in a control case AB3 **(A, D, G)** and in AD cases IF1 **(B, E, H)** and VK16 **(C, F, I)**. Layers are indicated to the right of panel **A**. Sections are immunostained with antibodies anti-NeuN **(A–C)**, anti-PHF-Tau-AT8 **(D–F)** and anti-Aβ **(G–I)**. Note the intense labeling of PHF-Tau-AT8 positive neurons (E, F) and Aβ positive plaques (H, I) in AD cases, particularly in case VK16, and the lack of labeling in the control case. CA1: cornu ammonis field 1; EC: entorhinal cortex; SUB: subiculum; WM: white matter. Scale bar (in I): 4.4 mm in plots and 1 mm in A–I.

Figure 2. Correlative light/electron microscopy of layer II and III of the EC. Delimitation of layers is based on the staining pattern of 1 µm-thick semithin section, stained with toluidine blue **(A)**, which is adjacent to the block for FIB/SEM imaging **(B)**. **(B)** SEM image illustrating the block surface with trenches made in the neuropil (three per layer). Asterisks in A and B point to the same blood vessels, showing that the exact location of the region of interest was accurately determined. **(C)** SEM image showing the front of a trench made to expose the tissue and to acquire the FIB/SEM stack of images at the final magnification. Scale bar (in C): 70µm in A; 85µm in B; 3µm in C.

Figure 3. Identification of synapses in serial electron microscopy images obtained by FIB/SEM. (A) Image from layer II showing the neuropil from an AD case, with two synapses indicated (arrows) as examples of asymmetric (AS, green) and symmetric synapses (SS, red). Synapse classification was based on examination of the full sequence of serial images; an SS can be visualized in **B–F**, and an AS in **G–K**. Scale bar (in K): 1,000 nm in A; 1,300 nm in B–K.

Figure 4. Proportions of the different synaptic shapes (A) in layers II (B) and III (C) of the EC in control subjects and AD patients. (A) Schematic representation of the synaptic shapes: macular synapses, with a continuous disk-shaped PSD; perforated

synapses, with holes in the PSD; horseshoe-shaped, with a tortuous horseshoe-shaped perimeter with an indentation; and fragmented synapses, with two PSDs with no connections between them. Proportions of macular, perforated, horseshoe-shaped and fragmented AS and SS are displayed for layer II **(B)** and III **(C)** of the EC in control subjects and AD cases. Statistical differences (indicated with asterisks) showed that in layer II, horseshoe-shaped AS were more frequent (χ^2, p=0.04) in AD cases; and in layer III of the AD group, fragmented (χ^2, p=0.0004) and macular (χ^2, p<0.0001) AS were more frequent, whereas perforated AS were less frequent in AD cases than in control individuals (χ^2, p <0.0001).

Figure 5. Analysis of the postsynaptic target distribution in layers II (A, B) and III (C, D) of the EC. (A) Schematic representation of the distribution of AS and SS on different postsynaptic targets from control cases in layer II. **(B)** Schematic representation of the distribution of AS and SS on different postsynaptic targets from AD patients in layer II. **(C)** Schematic representation of the distribution of AS and SS on different postsynaptic targets from control cases in layer III. **(D)** Schematic representation of the distribution of AS and SS on different postsynaptic targets from AD patients in layer III. In both layer II and layer III, the AS preferentially targeted spine heads, while the SS preferentially targeted dendritic shafts (asterisks; χ^2, p<0.0001). Percentages of postsynaptic targets are indicated, showing —from left to right— the most frequent type (AS on dendritic shafts) to the least frequent type (SS on spine necks). Synapses on spines have been sub-classified into those that are established on the spine head and those established on the neck.